Interaction of the Ekman Layer with Vortical Flow in a Short Couette-Taylor Cell

Olivier Czarny,*[1] Eric Serre,[1] Patrick Bontoux,[1] and Richard M. Lueptow[2]

[1]LMSNM, CNRS - Universités d'Aix-Marseille, IMT, La Jetée-Technopôle de Château-Gombert, 38 rue Frédéric Joliot-Curie, 13451 Marseille cedex 20, France.
[2]Department of Mechanical Engineering, Northwestern University, Evanston, IL 60208 USA.
e-mail: bontoux@l3m.univ-mrs.fr, r-lueptow@northwestern.edu

ABSTRACT

The endwalls in a cylindrical Couette flow cell introduce Ekman boundary layers that interact with the centrifugal instability. We investigate this interaction for both the rotor-stator configuration and for counter-rotating cylinders via direct numerical simulation using a spectral method. We consider a radius ratio of $\eta = 0.75$ in a short annulus having a length-to-gap ratio of $\Gamma = 6$. To analyze the nature of the interaction between the vortices and the endwall layers, several endwall boundary conditions were considered: fixed endwalls, endwalls rotating with the inner cylinder, endwalls rotating with the outer cylinder (for counter-rotating cylinders), and stress-free endwalls. Below the critical Taylor number in the rotor-stator case, endwall vortices for rotating endwalls are more than twice the strength of the vortices for fixed endwalls. Except for stress-free condition, the endwall vortices reduce the sharpness of the bifurcation diagram based on the radial velocity near the center of the annulus. The endwall conditions also have a strong effect on wavy vortex flow in the rotor-stator case, changing the number of vortical rolls and azimuthal waves. In some cases, there is evidence that the endwalls suppress the waviness to some extent. For counter-rotating cylinders, the role of the endwall boundary condition is more complex. Some endwall conditions tend to stabilize the structure of the flow, while in other endwall conditions tend to make the flow more disordered.

INTRODUCTION

The study of the centrifugal instability of the shear flow between differentially-rotating, concentric cylinders provides insight into flow stability and low-dimension bifurcation phenomenon. In most cases, the effects of the bounding endwalls on the flow are avoided. In theoretical studies the cylinders are assumed to be infinitely-long; in experimental studies the cylinders a made long compared to the gap between the cylinders; and in computational studies periodic boundary conditions are used to avoid endwall effects. Here we specifically consider the interaction between the boundary-driven flows at the endwalls and the centrifugal instability in the Taylor-Couette configuration. In particular, we focus on the effect of endwall vortices on the bifurcation from stable to vortical flow and the effect of the endwalls on the vortex structure in wavy vortex flow for the rotor-stator case. In addition, we consider the effect of endwalls for a variety of wavy and spiral flows in the case of counter-rotating cylinders.

In the cylindrical Couette configuration, the stable flow is geostrophic, so that the centrifugal force is balanced by the pressure gradient far from the endwalls. Below the critical conditions where the flow becomes centrifugally unstable, the no-slip boundary condition at the endwalls upsets the geostrophic force balance near the endwalls resulting in a radial velocity along the endwalls and a vortical structure that can propagate from the endwalls toward the center of the length of the annulus [1-3]. Above the critical Reynolds number, Taylor vortices replace the boundary-driven Ekman vortices and fill the annulus, but the sense of rotation of the vortical structure initiated by the Ekman vortices is maintained, even for relatively long cylinders. The cases of wavy vortex flow and counter-rotating cylinders are more complex.

We used direct numerical simulation to study the unstable flow between short, finite-length cylinders in both the rotor-stator and the counter-rotating configurations. This allows us to consider a variety of vortical flows in which the position and degree of the centrifugal instability vary. By using the various endwall conditions, we attempt to understand the interaction between the vortical flow due to the centrifugal instability and the Ekman endwall boundary layer flow.

DIRECT NUMERICAL SIMULATION

The configuration that is considered is an annular cavity between two concentric cylinders of inner and outer radii r_i^* and r_o^*, respectively, that rotate independently at Ω_i and Ω_o. The flow is described by the incompressible 3D Navier-Stokes equations written using cylindrical variables (r^*, z^*, θ) according to the velocity-pressure formulation. Parameters characteristic of the physical problem are the Reynolds numbers $Re_i = \Omega_i r_i^* d / \nu$ and $Re_o = \Omega_o r_o^* d / \nu$, the radius ratio $\eta = r_i^* / r_o^*$, and the aspect ratio $\Gamma = 2h / d$ where $d = r_o^* - r_i^*$. We consider four endwall conditions, depending on the rotation of the endwall, Ω_e: 1) stationary endwall (Ω_e=0); 2) rotation of the endwall with the inner cylinder (Ω_e=Ω_i); 3) rotation of the endwall with the outer cylinder (Ω_e=Ω_o); and 4) a stress-free boundary condition on the endwall, which is equivalent to a free surface (designated Ω_e=F).

The solutions to the Navier-Stokes equations are computed using a pseudo-spectral Fourier-Chebyshev collocation method taking advantage of the orthogonality properties of Chebyshev polynomials and providing exponential convergence. The time scheme is semi-implicit and second-order accurate. It is a combination of the second-order backward implicit Euler scheme for the time term, an explicit Adams-Bashforth scheme for the non-linear terms, and an implicit formula for the viscous diffusion term. The simulations for the transition to Taylor vortex flow are two-dimensional, while the simulations for wavy vortices and counter-rotating cylinders are three-dimensional. Details of the simulations are provided elsewhere [4,5].

RESULTS AND DISCUSSION

Consider first the case of endwalls fixed (Ω_e = 0), shown in Fig. 1. Even well below the transition to Taylor vortex flow ($\varepsilon = Re_i/Re_{i,crit} < 1$), the inward flow at the endwalls induces a strong endwall vortex with substantially weaker near the center of the annular length. As ε increases, the vortices near the center grow in strength. Above the transition ($\varepsilon > 1$), the vortices near the center grow in strength, eventually growing somewhat stronger than the endwall vortex. For all vortices, the maximum radial velocity is about 3 - 4 % of the surface speed of the inner cylinder. This suggests that while the mechanism that generates the vortices is quite different for Ekman vortices and Taylor vortices, the geometry of the situation, specifically the gap width d, and the inherent velocity scale in the problem ($r_i\Omega_i$) determine the magnitude of the velocity for the vortices. The thickness of an endwall boundary layer should scale as $\delta_E / L \sim Ek^{1/2} = (\nu/\Omega L^2)^{1/2}$ according to the theory for Ekman layers [6] indicating an endwall boundary layer thickness of 0.19 d, assuming that the significant length scale is $L = d$. The computational results indicate that δ_E ranges from 0.23 d for $\varepsilon < 1$ to 0.29 d for $\varepsilon > 1$. Similar results occur for $\Omega_e = \Omega_i$, except that the Ekman flow is stronger and directed toward the outer cylinder. For stress-free endwall conditions (Ω_e = SF), vortices appear only for $\varepsilon > 1$, since Ekman vortices do not form. For mixed boundary conditions ($\Omega_e = \Omega_i$ at the lower endwall and Ω_e = SF at the upper endwall), the vortices propagate from the lower endwall to the upper endwall as ε increases.

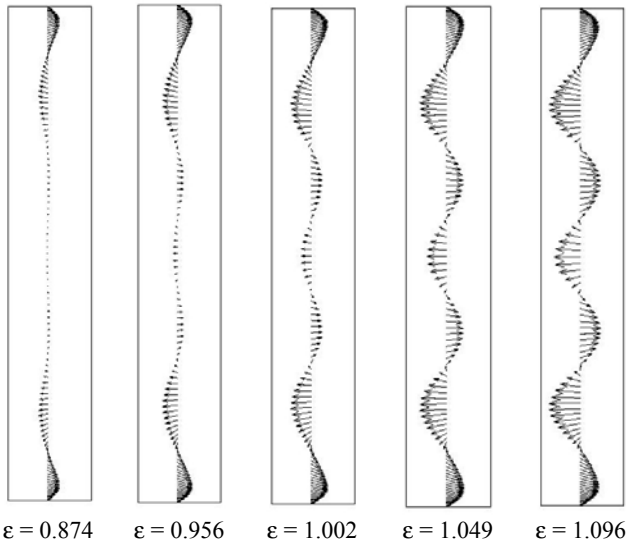

Fig. 1: Velocity vectors midway across the annular gap near the transition from nonvortical to vortical flow for $\Omega_e = 0$. The inner cylinder is the right vertical line.

It is clear that the endwall conditions affect the nature of the bifurcation at the transition from nonvortical to vortical flow. We examine the bifurcation by considering the maximum radial velocity near the center of the axial length of the annulus as a function of ε, as shown in Fig. 2. Depending on the endwall boundary conditions, the inflow and outflow boundaries occur either at the midpoint of the axial length or approximately d above or below the midpoint. Considering first the inset in Fig. 2, it is clear that except for the case of both

endwalls being stress-free, the endwall vortices reduce the sharpness of the bifurcation. The only case where the bifurcation is sharp is that for a stress-free endwall, consistent with previous predictions [7]. From the entire range of ε, it is clear that above the transition to vortical flow, the radial velocity at the inflow boundaries is only about 60% of the magnitude of the radial velocity at the outflow boundaries and that the radial velocity at outflow boundaries collapse onto a single curve, regardless of the endwall condition.

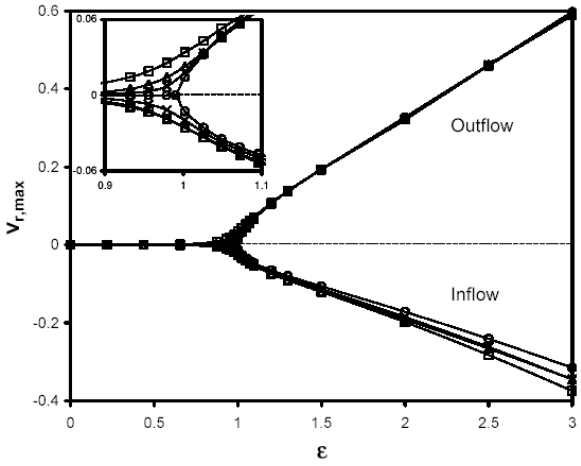

Fig. 2: Bifurcation diagram based on the maximum radial velocity nondimensionalized with $\Omega_i r_i^*$ at outflow regions and inflow regions near the axial center of the annulus. Δ, $\Omega_e = 0$; □, $\Omega_e = \Omega_i$; ○, $\Omega_e = F$ both endwalls; x, mixed endwall conditions.

We consider next the effect of the endwall conditions on wavy vortex flow, with an emphasis on the structure of the flow in the center of the annular length and near the endwalls. To obtain wavy vortex flow for rotating endwalls, a $m = 5$ (five azimuthal modes) perturbation was imposed on an initial condition of axisymmetric flow at $\varepsilon = 8$. The resulting steady-state flow had two azimuthal waves (m=2) and six vortical rolls including two large Ekman vortices adjacent to each endwall, as shown in Fig. 3a. A surface at an azimuthal velocity of $v_\theta/r_i\Omega_i = 0.48$ is shown in the figure, with the color indicating the radial velocity, $v_r/r_i\Omega_i$. Each of the two ridges in the center of the annulus represents outflow region between counter-rotating vortices. Thus, there are two vortices between the ridges. The $m = 2$ waviness is evident in the ridges. The large surface at each end of the annulus represents the strong azimuthal velocity in the Ekman rolls near the rotating endwall. Here the azimuthal waviness is suppressed, presumably because of the endwalls.

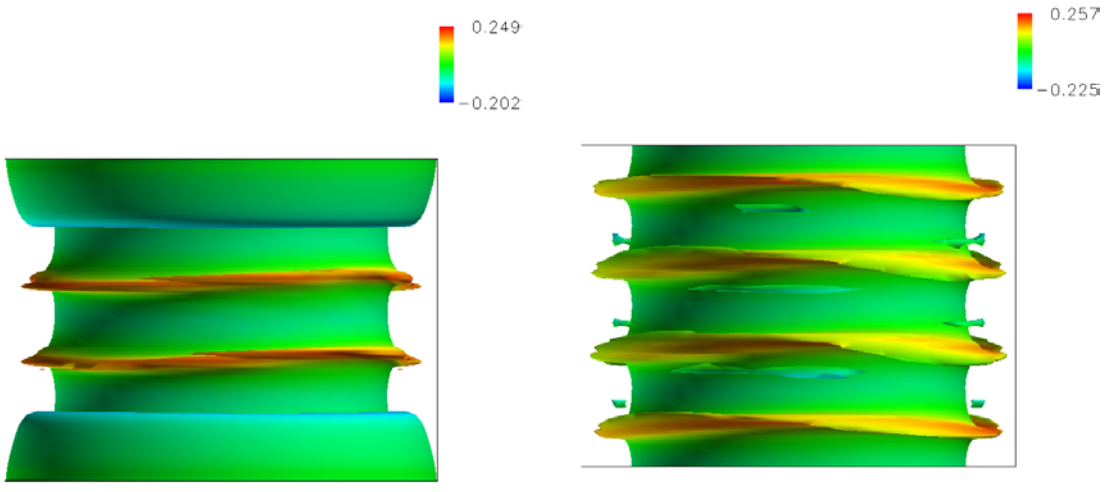

a **b**

Fig. 3: Isosurfaces of $v_\theta/r_i\Omega_i = 0.48$ with color showing $v_r/r_i\Omega_i$ at $\varepsilon = 8$. a) Endwalls rotating at $\Omega_e = \Omega_i$. b) Stress-free endwalls.

To obtain a wavy flow with stress-free endwalls, it was necessary to first compute the flow for fixed endwalls starting from the case shown in Fig. 3a resulting in $m = 2$ waviness with eight rolls. Using that flow as an initial condition, the endwalls were made stress-free resulting in a flow with eight rolls and $m = 2$, shown by the $v_\theta/r_i\Omega_i = 0.48$ surfaces of Fig. 3b. Again the ridges represent outflow regions, so that there are two rolls between ridges and a single roll above or below the ridges nearest the endwalls. Because of the stress-free condition, the endwall vortices are fairly similar to the vortices in the center of the annulus, in contrast to the case of rotating endwalls, where the endwall vortices are much longer in the axial direction. Surprisingly, the waviness on the side of the endwall vortices nearest the center of the annulus is not suppressed by the endwalls.

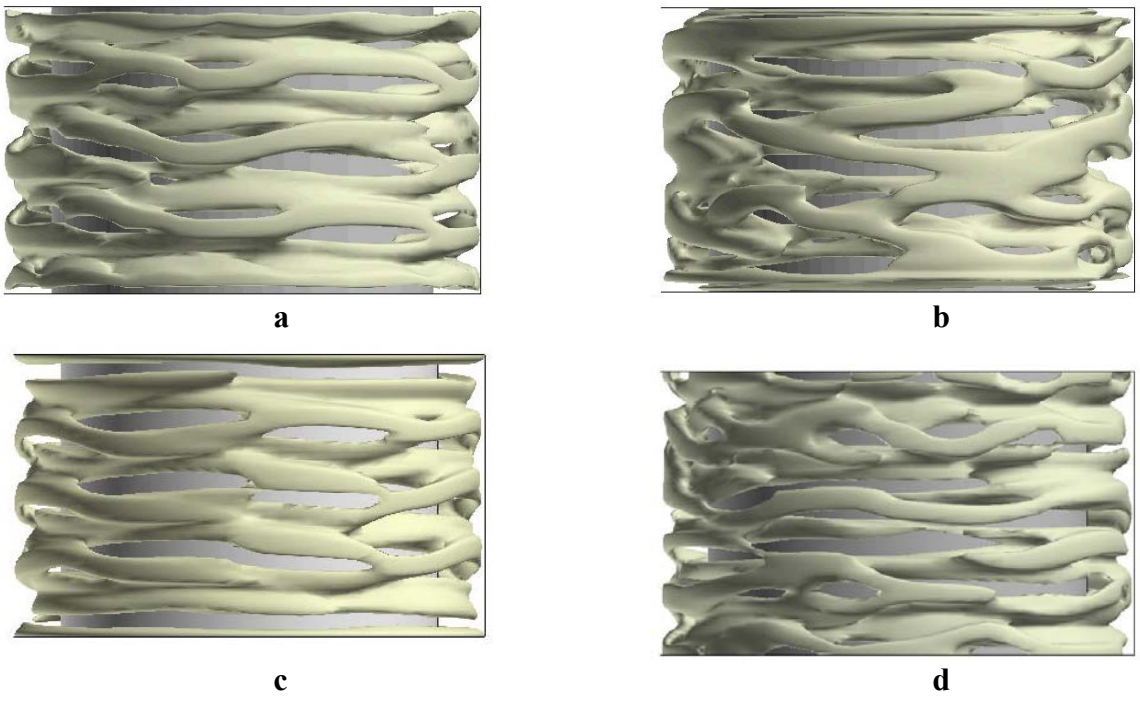

Fig. 4: Surfaces of $v_r/r_o\Omega_o = -2.33 \times 10^{-3}$ for various endwall conditions with R_i=375 and R_o = -500. a) $\Omega_e = \Omega_i$; b) $\Omega_e = \Omega_o$; c) $\Omega_e = 0$; d) Ω_e = SF.

Finally, we consider the case of counter-rotating vortices with various endwall conditions. Although we have considered several conditions, we show results here for an inner cylinder Reynolds number of Re_i = 375 and an outer Reynolds number of Re_o = -500. These conditions result in wavy interpenetrating spirals (WIS), which are most readily visible when plotting surfaces of radial velocity v_r, as shown in Fig. 4. The nature of the vortical flow depends on the endwall conditions. For the endwall rotating with the inner cylinder (Fig. 4a) and fixed (Fig. 4c), the flow is more ordered with smooth isosurfaces and regular intersections of surfaces compared to the endwall rotating with the outer cylinder (Fig. 4b) or a stress-free endwall condition (Fig. 4d). In the first case ($\Omega_e = \Omega_i$), there are 4 pairs of vortices having similar strength with one member of the pair closer to the inner cylinder and the other closer to the outer cylinder. In the second case ($\Omega_e = 0$), all of the vortices are nearer the inner cylinder. When the endwall rotates with the outer cylinder (Fig. 4b) or a stress-free boundary condition is applied to the endwalls (Fig. 4d), the flow is less ordered. For $\Omega_e = \Omega_o$, the vortices vary substantially in their strength around the circumference. For stress-free conditions, the vortices are stronger. The endwall vortices also differ substantially from case to case. For the endwall rotating with the inner cylinder, there is a strong, flat vortex near the endwall; for the endwall rotating with the outer cylinder, there is a weak vortex near the outer cylinder; for a fixed endwall, the vortex near the endwall rotates opposite the Ekman flow; and for the stress-free endwall, the vortex structure at the endwall varies substantially with azimuthal position.

REFERENCES

[1] G. Pfister, I. Rehberg. *Space-dependent order parameter in circular Couette flow transitions*, Phys. Lett., 83A, 19-22, 1981.

[2] G. Ahlers, D.S. Cannell. *Vortex-front propagation in rotating Couette-Taylor flow*, Phys. Rev. Lett., 50, 1583-1586, 1983.

[3] M. Lücke, M. Mihelcic, K. Wingerath. *Front propagation and pattern formation of Taylor vortices growing into unstable circular Couette flow*, Phys. Rev. A, 31, 396-409, 1985.

[4] O. Czarny, E. Serre, P. Bontoux, R.M. Lueptow. *Spiral and wavy vortex flows in short counter-rotating Taylor-Couette cells*, Theoret. Comput. Fluid Dynamics, 16, 5-15, 2002.

[5] O. Czarny, E. Serre, P. Bontoux, R.M. Lueptow. *Interaction between Ekman pumping and the centrifugal instability in Taylor-Couette flow*, Phys. Fluids, 15, 467-477, 2003.

[6] H.P. Greenspan. *The Theory of Rotating Fluids*, Cambridge University Press, London, 1969.

[7] K.A. Cliffe, J.J. Kobine, T. Mullin. *The role of anomalous modes in Taylor-Couette flow*, Proc. Roy. Soc. Lond. A, 439, 341-357, 1992.